Journal of Materials Chemistry A

Accepted Manuscript

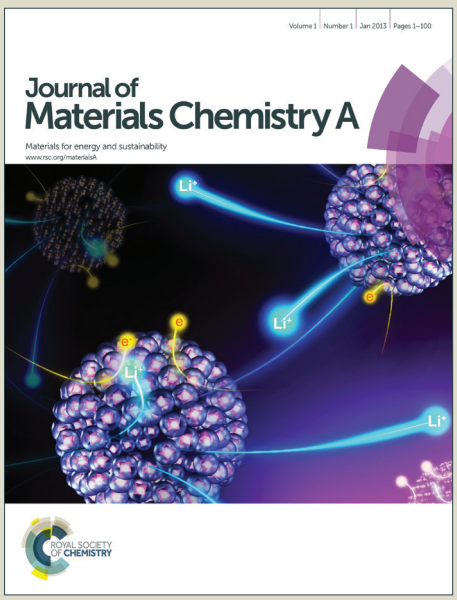

ROYAL SOCIETY OF CHEMISTRY

www.rsc.org/materialsA

Cite this: DOI: 10.1039/c0xx00000x

www.rsc.org/xxxxxx

ARTICLE TYPE

Highly sensitive H_2S detection sensor at low temperature based on hierarchically structured NiO porous nanowall arrays

Tingting Yu, XiaoLi Cheng, Xianfa Zhang, Lili Sui, Yingming Xu*, Shan Gao, Hui Zhao, Lihua Huo*

Received (in XXX, XXX) Xth XXXXXXXXX 200X, Accepted Xth XXXXXXXXX 200X

DOI: 10.1039/b000000x

3D network-like, hierarchically structured, porous nanowall NiO arrays were grown in-situ on ceramic tubes by a facile but environmentally friendly hydrothermal reaction with a subsequent calcined process. The arrays were constructed of the interconnected porous nanosheets, which were further assembled with abundant nanoparticles. The gas-sensing properties of such porous nanowall NiO arrays film sensor were investigated with eight inorganic and organic gases. The H_2S-sensing performance was observed with a large dynamic range (1 ppb-100 ppm) and the lowest detection limit of 1 ppb at 92 ^oC compared with other reported oxide-based sensors. The sensor exhibited not only high sensitivity, good selectivity and reproducibility to H_2S with resistance to humidity at low temperature of 92 ^oC and room temperature, but also good linear relationship under concentration ranges of ppm level (1-100 ppm) and ppb level (1 ppb-1 ppm). The excellent sensing performance of this arrays film sensor to H_2S could be ascribed to the porous structures in the unique nanowall arrays with a large specific surface area, which benefit H_2S molecules to adsorb/desorb onto/from the arrays surface as well as the electrons transfer. The formation of NiO arrays and its possible H_2S-sensing mechanism were discussed in detail.

Introduction

Hydrogen sulfide (H_2S) is an extremely toxic and dangerous gas due to its flammability and high lipid solubility, which allows it to pass through the cellular membranes and to form a complex bond with iron in the mitochondrial cytochrome enzymes, thus preventing cellular respiration. According to the U.S. Scientific Advisory Board on Toxic Air Pollutants recommendation, the acceptable levels of H_2S in the ambient environment are reported to be within the range < 83 ppb [1]. Therefore, early recognition and real time detection within this concentration range of H_2S is crucial to protect people away from disease. At present, typical gas sensors for detection of hydrogen sulfide are electrochemical sensors [2], optical sensors [3, 4] and chemical sensors [5, 6]. Among the above sensors, chemical sensors based on metal oxide semiconductors have attracted a great attention owing to the high sensitivity, excellent stability, fast recovery time and simplicity in fabricating sensors. Up to now, a few kinds of metal oxide-based nanostructured sensing materials have been reported for detection of ppb-level H_2S (≤ 100 ppb), including CuO [7, 8], CuO-SnO_2 [9, 10, 11], WO_3 [12], In_2O_3 [13] and ZnO [14]. Most of the materials exhibited low gas response (R_a/R_g or R_g/R_a < 2) to tens of ppb H_2S even at the temperature of higher than 150 ^oC. Although the sensors based on In_2O_3 nanoparticles [13] and ZnO nanorods [14] could accomplish detection of H_2S at room temperature, the gas responses of which were only 0.5 (20 ppb) and 1.7 (50 ppb), respectively. Only the CuO-SnO_2 hollow spheres [11], constructed of numerous nanoparticles, showed high response to 10 ppb H_2S at room temperature. Among the above H_2S sensing materials, only hierarchically porous CuO hollow spheres [7] showed the lowest detection limit of 2 ppb, while the others exhibited detection limit of H_2S in the range of 10 ~ 100 ppb. Therefore, it is still necessary to investigate ppb-level of H_2S detection material with high gas response and marked selectivity at low working temperature.

As one of the most important p-type metal oxide semiconductor, nickel oxide with relatively wide band gap (Eg=3.6-4.0 eV) and excellent electrical properties, has been used in H_2S gas detection. Thick film sensors of NiO nanoparticles [15] exhibited good response to 100 ppm H_2S at 150 ^oC. The sensing performance of NiO sensors could be enhanced by the incorporation of noble metal (Au@NiO yolk–shell [16]) and metal oxide (Fe_2O_3-loaded NiO nanoplate [17] and NiO@ZnO heterostructured nanotubes [18]), and fabrication of thin film sensor (NiO nanoparticle films [19]). However, the relatively high working temperature (> 150 ^oC), especically high detection limit (> 1 ppm) of these sensors still need to be further improved in order to satisfy the acceptable detection level of H_2S in indoor air quality monitoring. In recent years, the gas sensors based on hierarchically structured semiconductors, especially the in-situ growth of hierarchically structured materials showed more significant gas sensing property. For example, the 3D hierarchical ZnO flowers sensors assembled with spiderweb-like architectures [20] exhibited an improved sensing performance to ethanol, including low working temperature (decrease to room temperature), low detection limit (down to ppb level), short response and recovery times (lower to sub-second) in comparison to the thick film sensor. Just recently, Hosseini et al [21] reported

that the aligned ZnO nanorods arrays with flower-like structure could detect H_2S in 500 ppb level at room temperature. It means that in-situ growth of gas sensors based on unique, uniform and stable hierarchical micro-nanostructures or well-defined/ordered arrays could be designed with superior sensing property, due to their more gas diffusion routes, easy electron transfer, large specific surface area and more effectively active sites. If NiO was designed as such configured sensor, it possibly could decrease the detection limit and lower the working temperature of NiO sensors to H_2S gas. At present, NiO films with similar structure of mesoporous NiO nanosheet networks [22] and hierarchical NiO nanosheets [23] have been prepared by hydrothermal/solvothermal method and applied in supercapacitors and Li ion batteries.

Herein, we report a simple fabrication route of 3D network-like, hierarchically structured NiO arrays, which are assembled with porous nanosheets grown in-situ onto a ceramic tube to form arrays sensor. The sensor exhibits better selective H_2S sensing characteristics against seven other gases and can detect ppb-level H_2S gas at low temperature of 92 ^oC and room temperature. It shows good linear relationship in the concentration ranges of 1 ppb-1 ppm and 1-100 ppm.

Experimental

Preparation of NiO nanowall arrays

Nickel sulfate ($NiSO_4 \cdot 6H_2O$) and aqueous ammonia (25%) were purchased from Tianjin Chemical Group Co. Ltd. All of the reagents involved in the experiments were of analytical reagent (AR) grade (purity > 99%) and were directly used without further purification. All of the ceramic wafers and ceramic tubes used in this study were carefully cleaned by deionized water (18.2 MΩ), ethanol and acetone in ultrasonic bath before use.

NiO nanowall arrays were obtained via heat treatment of $Ni(OH)_2$ precursor which was synthesized by hydrothermal reaction described as follows: $NiSO_4 \cdot 6H_2O$ (2.66 mmol) was dissolved in 30 mL of deionized water. After dropping 1 mL of ammonia liquor (4.7 $mol \cdot L^{-1}$), a clear grass-green color solution was obtained after continuously magnetic stirring for 1 h. The above solution and the ceramic wafers were transferred into a Teflon-lined stainless-steel autoclave with a capacity of 50 mL and maintained at 200 ^oC for 5 h. After cooled down to room temperature, $Ni(OH)_2$ precursors on the ceramic wafers were swilled with deionized water and ethanol for several times and dried at 70 ^oC for 12 h. Finally, NiO porous nanowall arrays were obtained by calcination of the precursors at 500 ^oC for 2 h in air.

Characterization of materials

The phase and crystallization of the products were characterized by X-ray powder diffraction (XRD) using advanced X-ray diffractometer (D8 ADVANCE, BRUKER, Germany) in a 2 theta range from 5 to 80 degree with Cu-Kα radiation (λ=0.154056 nm). The morphology and refinement structure of the products were obtained by scanning electron microscopy (SEM, S-4800, HITACHI, Japan), transmission electron microscopy (TEM, JEOL-JEM-2010, Japan), high-resolution transmission electron microscopy (HRTEM) and selected area electron diffraction (SAED) analyses. The Raman spectra of the products were recorded using a Renishaw 1000 Micro-Raman spectrometer with a long-range 50 × objective, 10S integration, and 10% laser power (457.9 nm excitation; 8 mW at 100%). X-ray photoelectron (XPS) spectra were obtained on a VG ESCALAB-MK photoelectron spectrometer with Al Kα as the excitation source. The binding energy values were corrected for specimen charging by referencing the C 1s line to 284.6 eV. The specific surface area and pore size distribution were calculated from a nitrogen adsorption-desorption analysis conducted at 77 K using Brunauer-Emmett-Teller method (BET, Tristar 3020, Micrometrics, USA). The gaseous product after the NiO nanowall arrays sensor exposed to H_2S was monitored by gas chromatography-mass spectrometer (GC-MS, AGILENT, 6890-5973N) using a DB-5 (30 m × 0.25 mm × 0.25 μm, AGILENT) column from 50 to 250 °C at a heating rate of 10 °C min^{-1} in N_2 flow rate of 1 mL min^{-1}.

Fabrication of the sensors and measurement of gas sensing properties

In-situ deposited NiO porous nanowall arrays film sensors (named as arrays film sensors) were fabricated via the same conditions for NiO film preparation, except that the ceramic wafer substrate was replaced by ceramic tube, on which Au electrodes were pre-deposited. Thick film sensors were also fabricated according to Ref. [24] which was also given in Supporting information for comparison with the gas sensing property of arrays film sensors. Then Ni-Cr heating wire was employed as a heater of the sensors passing through the tube to control the operating temperature. Through the solder, the ceramic tube and heating wire were connected to the base. To improve their stability and repeatability, the gas sensors were all aged at 300 ^oC for 3 days in air.

The sensing properties of the sensors were performed by the JF02E gas sensing measurement system (Sino-platium Metals CO. Ltd, China). The static test method was used to measure the sensing property, the gas concentration was controlled through adding different quantity of test gases in container and the testing principles of the above gas sensors were similar to those of other oxide gas sensors that described in the literature [24]. Detailed explanation for trace H_2S gas measurement was shown in Supporting information and the schematic drawing of gas sensing set-up was provided in Fig. S1. The working temperatures of sensors were adjusted by varing the heating voltage (V_H) of the sensor. The relative humidity (RH) of the environment during the measurement was about 25 %. The gas response (S_r) of sensors for the test gases is defined as the ratio of R_g/R_a, where R_g and R_a are the resistances of sensors in target gases and air, respectively. The selectivity coefficient (K_{AB}) of A gas to B gas is defined as S_A/S_B, where S_A and S_B are the responses of sensors measured in A gas (hydrogen sulfide in this study) and in interfering gases (acetone, chlorobenzene and other gases in this study). The time taken by the resistance change of sensors to 100 s is defined as the response time, when the sensor is exposed to the target gas. The time taken by the resistance change of sensors from R_g to R_g - 63 % (R_g - R_a) is defined as the recovery time, when the sensor is retrieved from the target gas.

The humidity sensing properties of NiO nanowall arrays film sensor were also studied using different saturated salt solutions. Relative humidity conditions of 94%, 75%, 54%, 33%, 23% and 11% were obtained by saturated solutions of KNO_3, NaCl, $Mg(NO_3)_2$, $MgCl_2$, CH_3COOK and LiCl, respectively. Each of

the saturated salt solution was kept in the glass chamber at least for 24 h before the sensing measurement. The humidity response measurements of the sensors were carried out at room temperature and 92 °C, respectively. The humidity response (S_H) is defined as the ratio of resistance of the sensor in the test humidity (t %) to that in air.

Results and discussion

Fig.1a shows the XRD patterns of the as-prepared precursor and the calcined product, which are presented in log scale because of the weak diffraction intensity of the samples. The precursor obtained from hydrothermal synthesis at 200 °C for 5 h exhibits similar XRD pattern of the $Ni(OH)_2$ phase (JCPDS 03-0177, $P\bar{3}m1$, a=0.3114 nm, b=0.3114 nm, c=0.4617 nm). Namely, all the diffraction peaks appearing at 19.4, 33.5 and 38.8° can be indexed to the lattice planes of (001), (100) and (101) of $Ni(OH)_2$, respectively. After the precursor was calcined at 500 °C for 2 h, all the diffraction peaks of the calcined product can be attributed to those of NiO phase (JCPDS 04-0835, $Fm\bar{3}m$, a=0.4177 nm, b=0.4177 nm, c=0.4177 nm). The two peaks at 37.3 and 43.5° match well with the (111) and (200) planes of NiO, respectively. The positions of the diffraction peaks of the precursor and calcined product are all consistent well with the theoretical XRD data of $Ni(OH)_2$ and NiO, respectively. The widening of the diffraction peaks might be due to the influence of nanostructural effect and thinness of arrays film. In order to confirm the phase and purity of the arrays films, Fig. S2 shows the XRD patterns of the powder products precipitated on the bottom of autoclave under the same hydrothermal conditions and its calcined product. Well-crystalized phases of $Ni(OH)_2$ and NiO can be clearly seen, without any impurity. It indicates the existence of the pure NiO in the calcined arrays.

The microstructures of the precursor and calcined product were also obtained by micro-Raman spectra (Fig. 1b). The peak at 459 cm^{-1} of the precursor corresponds to the stretching vibration band of Ni-O(H) [25] and the peak at 520 cm^{-1} is attributed to defective or disordered $Ni(OH)_2$ [26]. For the calcined product, three Raman peaks located at about 560, 700 and 1085 cm^{-1} are observed, which can be assigned to the shaking vibration bands of NiO [27, 28]. The first one can be attributed to the first-order longitudinal optical phonon modes of NiO. The latter two can be assigned to second-order transverse optical and longitudinal optical phonon modes of NiO, respectively. These results are in accordance with those of XRD analysis.

SEM images of products grown on ceramic wafers are presented in Figure 2a-d. Regularly grown network-like structure of $Ni(OH)_2$ precursor can be seen from the low magnification SEM image (Fig. 2a) which is also called as nanowall arrays. High magnification image (Fig. 2b) further shows that the arrays are composed of interconnected thin nanosheets. After calcination (Fig. 2c-d), the obtained NiO product retain the hierarchical structure morphology of the precursor. And the insets of high magnification images (insets of Figs. 2b, d) confirm that the surfaces of nanosheets, including the products before and after calcination, are smooth, and the thickness is about 14 nm.

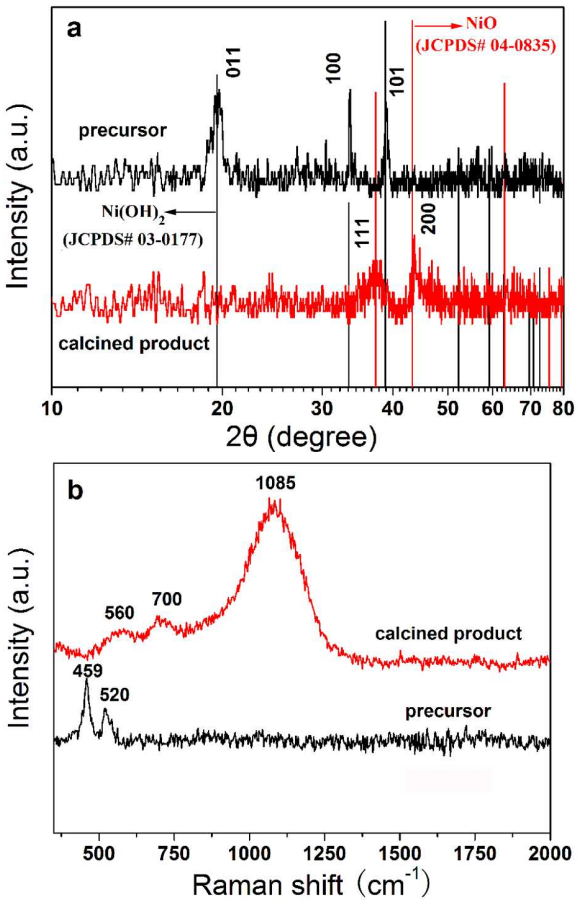

Fig. 1 XRD patterns (a) and Raman spectra (b) of the as-prepared precursor and the calcined product after heat treatment at 500 °C for 2 h in air.

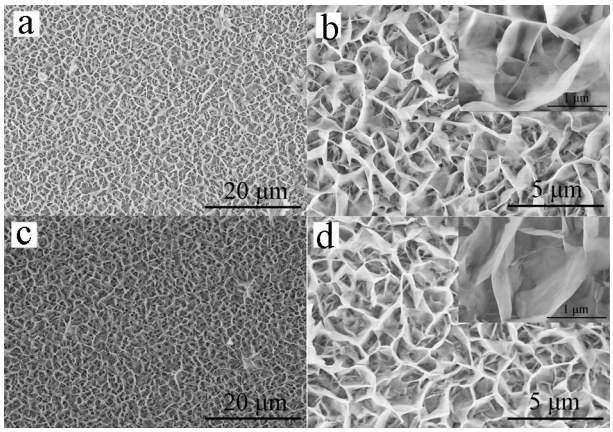

Fig. 2 SEM images of $Ni(OH)_2$ nanowall arrays (a and b) and NiO nanowall arrays (c and d) grown on the ceramic wafers.

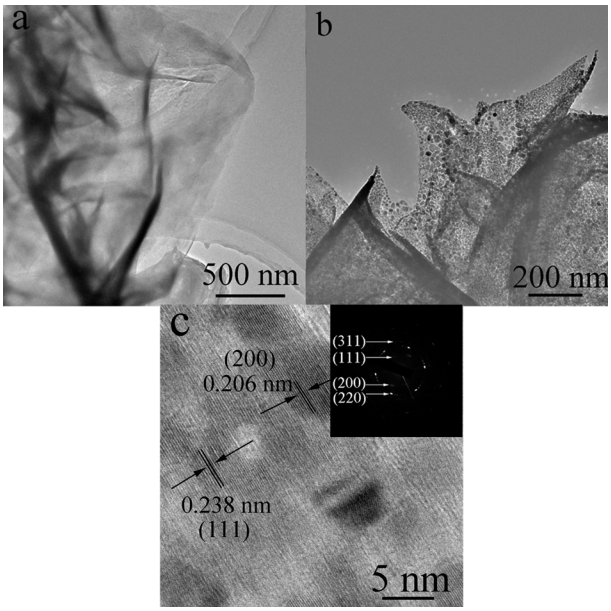

Fig. 3 TEM (a) image of the $Ni(OH)_2$ nanosheets and TEM (b), HRTEM (c) images and SAED pattern (inset of c) of the NiO nanosheets.

In order to understand the microstructure of $Ni(OH)_2$ precursor and the heat-treated NiO product in more detail, TEM (Fig. 3a-c) images at high magnification were analyzed. It shows that the nanowall arrays of precursor are just constructed of the single and thin nanosheets, while the nanosheets in the calcined arrays are further assembled with abundant sub-nanometer of nanoparticles with a slick surface (Fig. 3b). That means the primary building blocks of precursor are nanosheets, but those of calcined product are nanoparticles. Porous structure is also observed in nanosheets of calcined product with pore size in a range of 5.7 to 27.1 nm, which are resulted from the stacking of nanoparticles. HRTEM image (Fig. 3c) from one nanosheet of calcined product displays clear lattice fringes with spacing of 0.206 nm and 0.238 nm, which can be attributed to the (200) and (111) lattice planes of NiO, respectively. The results are in good accordance with its XRD result (Fig.1). The corresponding SAED pattern (inset of Fig. 3c) of calcined product confirms that the NiO nanowall arrays are polycrystalline structures. The diffraction rings in the electron diffraction pattern can readily be indexed as (111), (200), (220) and (311) planes of the cubic NiO. This result further confirms the existence of nickel oxide phase in the calcined arrays film as XRD did.

The pore structure and specific surface area of the NiO nanosheets were also detected by nitrogen adsorption-desorption measurement, as shown in Fig. 4. It can be seen that the N_2 adsorption-desorption isotherms of NiO nanosheets display a type IV isotherm with a H3 type hysteresis loop according to the IUPAC classification. It indicates the presence of mesopores possibly formed by stacking of component nanoparticles. The corresponding Barrett-Joyner-Halenda (BJH) pore size distribution curve (inset of Fig. 4) shows that most of pores of NiO nanosheets fall into the size of 20-60 nm with a broad peak. The measured BET specific surface area of NiO nanosheets is 84.64 $m^2 \cdot g^{-1}$. Such NiO nanowall arrays are expected to show excellent gas-sensing performance due to their porous structures in the unique nanowall arrays with large specific surface area.

A plausible growth mechanism of the 3D network-like precursor nanowall arrays structure was studied in detail by SEM, based on the experimental conditions and the structural morphology of the nanosheets. Because the construction of hierarchical nanowall arrays was too fast under the hydrothermal temperature of 200 °C, 100 °C was chosen as the reaction temperature to see the detailed formation processes of nanowall arrays. The images of the intermediate products obtained at 100 °C from 1 min to 1 h during the hydrothermal reaction are shown in Fig. 5b-e. Fig. 5a shows the coarse surface of ceramic wafer. At the early stage of the hydrothermal reaction, the particles on the surface of ceramic wafer promote the formation of precursor nucleus, which provide energetically favorable sites for the formation of initial seed nucleus (Fig. 5b) as the hydrothermal reaction proceeds. Subsequently, these nucleuses grow and aggregate into relatively larger and regular nanoparticles after a sufficient density of nucleuses have formed, and parts of the nanoparticles form lamellar structure (Fig. 5c). After that, due to the tendency of thermodynamic stability, the formed nanoparticulates aggregates grow anisotropically along the preferential orientation, regularly

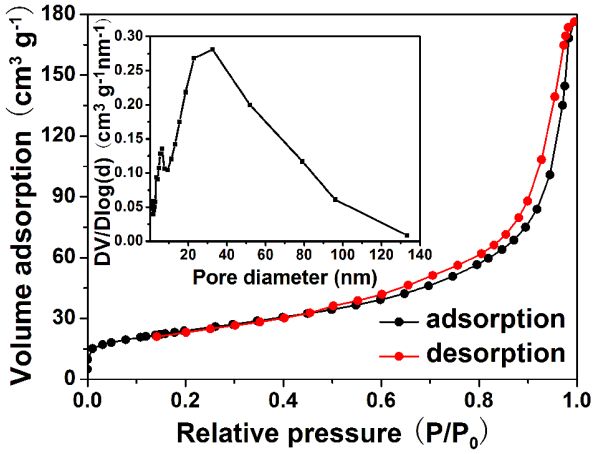

Fig. 4 Nitrogen adsorption-desorption isotherms and (inset) pore size distribution of the NiO nanosheets.

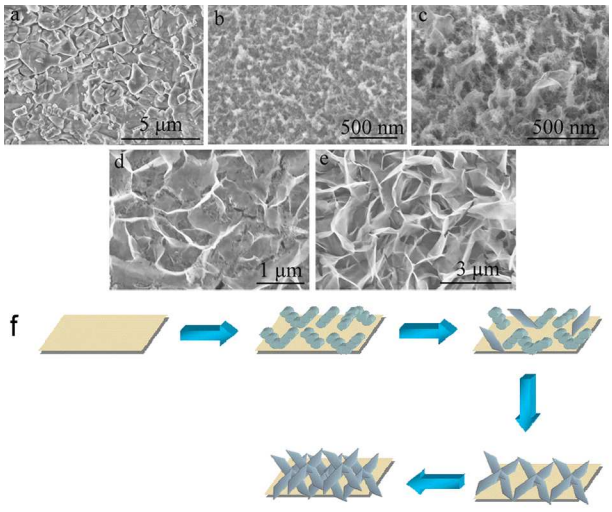

Fig. 5 SEM images of the ceramic wafer (a) and of the precursors samples obtained at different hydrothermal reaction durations at 100 °C : 1 min (b), 10 min (c), 30 min (d), 60 min (e) and schematic illustration of the formation mechanism of the precursor nanowall arrays (f).

stack with each other and form nanosheets with smooth surface (Fig. 5d). As the hydrothermal reaction further goes on, the nanostructures continue to grow and crystallize, and 3D network-like, hierarchical nanowall NiOH arrays gradually form which are composed of nanosheets with smooth surface (Fig. 5e). Fig. 5f shows the schematic illustration of the formation mechanism of the precursor nanowall arrays.

In order to investigate the effect of assembly method on the sensing property of NiO sensors, the morphology and sensing property of the in-situ deposited arrays film and thick film sensors are discussed as follows. Figs. S3a and b show the SEM images of the two sensors. The regularly arranged nanowall arrays are maintained on the substrate surface of the arrays film sensor. The surface of the thick film sensor is not regularly arranged, it is disordered and aggregated with smaller units of nanosheets. It indicates that the nanowall arrays were damaged completely during the thick film sensor fabrication. Fig. S4a shows the relationship between the gas responses and different working temperatures of two sensors to 10 ppm H_2S. The gas responses of the two sensors all increase with the increase of working temperature and approach a maximum value at 92 ^oC, gradually decrease with further increasing the temperature. The arrays film sensor shows a higher gas response at the same temperature and a lower detection limit comparing to the thick film sensor. The gas responses of both sensors to 10 ppm of H_2S are 12.9 (arrays film sensor) and 2.3 (thick film sensor) at 92 ^oC. The minimum detection limit of the arrays film sensor is 1 ppb, while that of the thick film sensor is 5 ppm. Figs. S4b and c display the response and recovery characteristics of two kinds of sensors to H_2S in the range of 1-100 ppm at 92 ^oC. The recovery time of the thick film sensor is about 455 s to 10 ppm H_2S, while that of the arrays film sensor is 79 s. The corresponding gas sensing measurements confirm that the assembly method of sensing material on the sensor could not affect the optimal working temperature of the sensors, but affect the response and recovery characteristics of the sensors to H_2S greatly. The difference of the sensing property of these two sensors could be attributed to the orderedly arranged nanosheets structure in the arrays film sensor, which is benefit for H_2S molecules to adsorb/desorb on the surface of arrays film and the transfer of electrons. Thus, the investigation of sensing property was focused on the NiO arrays film sensors in the following discussion.

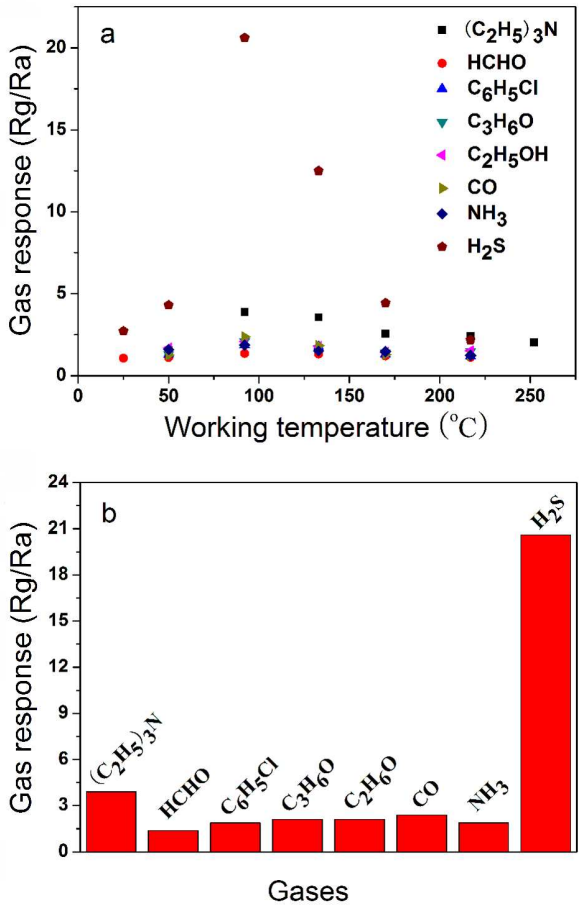

Fig.6 Responses of arrays film sensor versus 50 ppm of various gases at different working temperatures (a) and at the optimal working temperature of 92 ^oC (b).

The working temperature range is an important parameter for semiconductor oxide sensors to detect different target gases. Thus, the gas-sensing performances of NiO arrays film sensor towards 50 ppm different gases, including $(C_2H_5)_3N$, HCHO, C_6H_5Cl, C_3H_6O, C_2H_5OH, CO, NH_3 and H_2S, were investigated at the working temperature range from room temperature to 300 ^oC, as shown in Fig. 6a. It can be seen that the gas responses of the sensor to same concentration of different gases have the same change trend, the gas response increases with the increase of working temperature from room temperature, and approaches a maximum value at 92 ^oC, however, gradually decreases with further increasing the working temperature. 92 ^oC is named as the optimal working temperature of this NiO arrays film sensor. This is possibly attributed to the adsorption/desorption quantities of H_2S molecules on the sensing material. At low temperature (< 92 ^oC), a small amount of H_2S gas molecules adsorb on the surface which in turn react with the chemisorbed oxygen ions. When the arrays film sensor is exposed to H_2S gas at 92 ^oC, more H_2S gas molecules adsorb on the surface and react with O_2^- on the surface of NiO sensor. It suggests high reaction activity of the sensor surface at the optimal working temperature of 92 ^oC. However, with the temperature increasing, H_2S molecules desorb from NiO surface much easier, leading to the effective adsorption quantities of H_2S decrease. This results in the gas responses of NiO decrease from 92 to 300 ^oC [24]. The gas responses of the sensor to 50 ppm eight gases of triethylamine, formaldehyde, chlorobenzene, acetone, ethanol, carbon monoxide, ammonia and hydrogen sulfide, are 3.9, 1.4, 1.9, 2.1, 2.1, 2.4, 1.9 and 20.6, respectively, which were measured at 92 ^oC, as shown in Fig. 6b. The selectivity coefficients (K_{AB}) of H_2S gas to other gases are 5.3, 14.7, 10.8, 9.8, 9.8, 8.6 and 10.8, respectively, indicating an extremely sensitive and selective property of NiO nanowall arrays to H_2S gas at 92 ^oC. It is worthy to point out that the sensor also exhibits a good sensing property to H_2S gas at room temperature with a high response of 2.72. It indicates that the NiO nanowall arrays sensor has a quiet wider working temperature range to detect H_2S gas, especially suitable to work at low temperatures. This is very important for semiconductor oxide sensors to exhibit a good sensing property at lower working temperature, due to the demand of energy exhaustion decreasing.

The real-time gas responses of NiO sensor to different concentrations of H_2S gas at the optimal working temperature of 92 °C are shown in Fig. 7a. With the concentration of H_2S increasing, the gas responses of sensor increase in a good linear relationship (R^2=0.997) for a concentration range from 1 to 100 ppm, especially in the low concentration range from 1 ppb to 1 ppm (R^2=0.999). The sensor exhibits an excellent gas response of 2.1 to 10 ppb of H_2S with a detection limit of 1 ppb (response of 1.23), which is the lowest compared with other reported metal oxide-based sensors. It indicates that the present sensor can detect sub-ppb levels of H_2S and has good practical application to monitor the pollution of indoor air. The recovery times of the sensor to different concentrations of H_2S gas range from 49 s to 123 s, as shown in Fig. 7b. Obviously, the sensor exhibits a reversible response signal to H_2S gas in the desorption process. Taking into account all gas sensing characteristics such as gas responses, the operating temperature, selectivity and the minimum detection limit, the NiO porous nanowall arrays in the present study provide a novel and convenient solution to detect trace hydrogen sulfide, especially ppb-level H_2S, with minimum cross-responses to various interference gases.

Fig. S5a shows the responses of the NiO nanowall arrays film sensor to 10 ppm H_2S for 5 times of continue measurements at the working temperature of 92 °C. It indicates that the sensor maintains its initial response amplitude after five successive sensing tests, demonstrating better reproducibility of such NiO nanowall arrays film sensor to H_2S gas. To investigate the long-term stability of the arrays film sensor, the sensors were stored in air for subsequent sensing property tests after the first measurement. The sensor remains the original response to 10 ppm H_2S with changes less than 3 % after 60 days (Fig. S5b). It indicates that the arrays film sensor has a satisfying long-term stability.

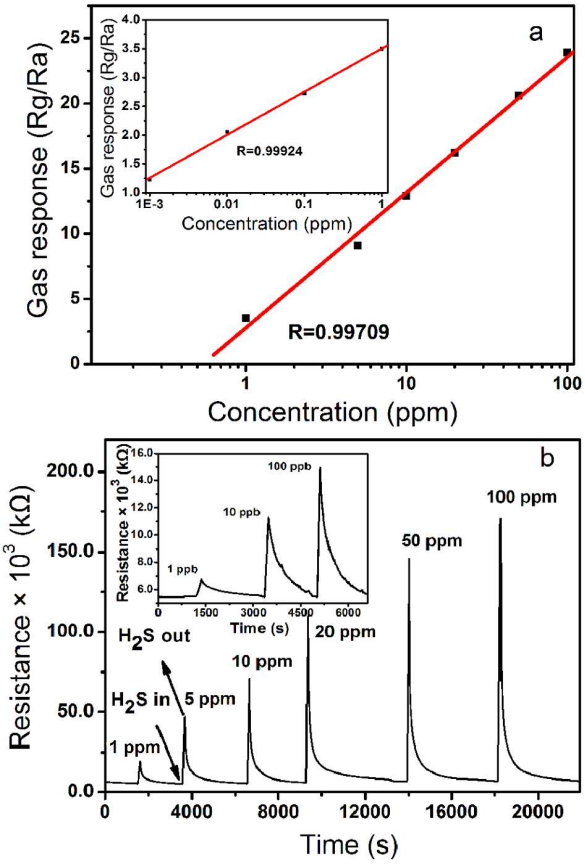

Fig.7 The relationship between the responses of NiO arrays film sensor and H_2S concentration (a) and the sensing transients of NiO arrays film sensor to different concentrations of H_2S (b).

Relative humidity (RH) in air plays an important role in determining the gas response of metal oxide-based gas sensors, especially when their working temperatures are at room temperature or low temperature. Hence the influence of relative humidity on this NiO arrays film sensor was also investigated, as shown in Fig. S6. It can be seen that there is a very small change of gas response when the sensor was put in different humidity atmospheres, suggesting that the relative humidity has almost no effect on the sensor. All the above results indicate that the NiO arrays film sensor is a good candidate for detection of low concentration of H_2S at low working temperature. The superior H_2S sensing performance of this sensor could be mainly attributed to the hierarchically porous structure and large specific surface area of such nanowall arrays film in-situ deposited on the sensor.

To illuminate the surface composition and the chemical state changes of the elements in the NiO nanowall arrays film sensor after exposure to H_2S, XPS measurements were carried out and the spectra are shown in Fig. 8. In order to explain the composition of the arrays film clearly, we first simply discuss typical survey and Ni 2p XPS spectra of the calcined powder (shown in Fig. S7). The survey spectrum of Fig. S7a involves distinct peaks at 530.6 (O 1s), 1013.5 (Ni 2s), 872.5 (Ni $2p_{1/2}$), 853.9 (Ni $3p_{3/2}$), 780.8, 714.1, 642.4 (auger electron peak of Ni), 113.8 (Ni 3s), 69.7 (Ni 3p) and 169.1 eV (S 2p). It indicates that the final product contains Ni, O, C and S elements. A small amount of sulfur element in the calcined product is from sulphate residue in raw material and carbon results from the standard carbon. From the Ni 2p XPS spectrum of NiO powder (Fig. S7b), it is observed that a main peak at 853.9 eV of Ni $2p_{3/2}$ with a satellite peak (860.8 eV), as well as a main peak at 872.4 eV and its satellite peak (879.4 eV) of Ni $2p_{1/2}$ correspond to Ni^{2+} in cubic rocksalt NiO [29, 30]. The shoulder peak at 855.8 eV might be attributed to the Ni^{2+} species on the powder surface [31, 32]. The energy separation between Ni $2p_{3/2}$ and Ni $2p_{1/2}$ is approximately 18.5 eV, indicating the well-defined symmetry of Ni^{2+} in oxide form [33]. In the case of the NiO arrays film sensor, the Ni 2p XPS spectrum before the sensor was exposed to H_2S is illustrated in Fig. 8a. The main peaks at 853.9 and 872.6 eV, the shoulder peak at 855.9 eV and two satellite peaks at 861.1 and 879.3 eV are consistent with the above values of pure NiO powder. The raised intensity of the shoulder peak (855.9 eV) might be related to the increase of Ni^{2+} species concentration on the film surface, which possibly resulted from hierarchically structured arrays film, constructed of thin nanosheets with porous structure. After the sensor was exposed to H_2S, it is found that the binding energies of Ni $2p_{3/2}$, Ni $2p_{1/2}$, the shoulder peak and two satellite peaks center at 854.0, 872.4, 856.0, 860.8 and 879.0 eV (Fig. 8b), respectively. The position and shape of Ni 2p peaks are similar with those of NiO arrays film before exposure to H_2S, which suggests that the valence state of nickel has no obvious change before and after the sensor exposure to H_2S.

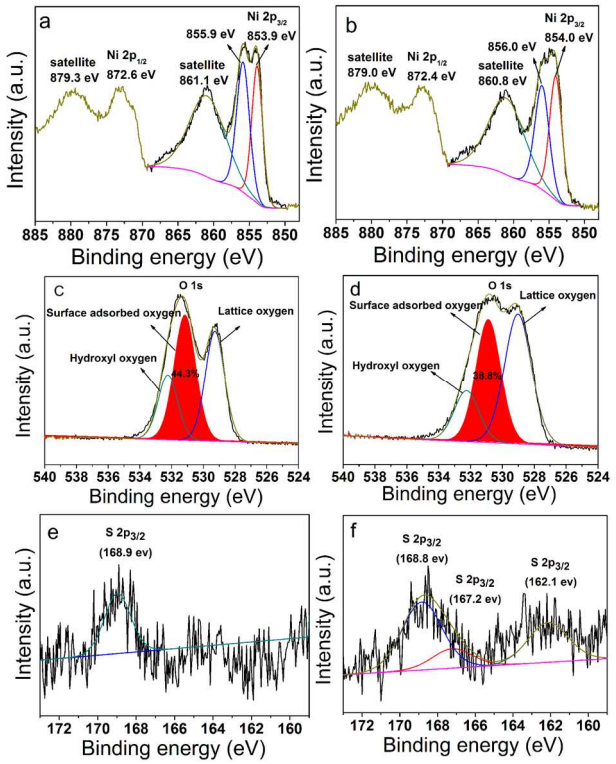

Fig. 8 Ni 2p (a, b), O 1s (c, d) and S $2p_{3/2}$ (e, f) XPS spectra of NiO nanowall arrays film sensor before (a, c, e) and after (b, d, f) exposure to H_2S at 92 °C.

Both of the O 1s spectra of NiO nanowall arrays film (shown in Figs. 8c and d) could be deconvoluted into three peaks at 532.2/532.2, 531.2/530.9 and 529.3/529.1 eV, assigning to the hydroxyl oxygen, surface adsorbed oxygen and lattice oxygen, respectively [20]. A higher percentage of surface adsorbed oxygen (44.3%) can be seen before the sensor exposure to H_2S, in comparison to that (38.8%) after the sensor reaction with H_2S. The surface adsorption oxygen decreases obviously when NiO arrays film sensor was exposed to H_2S, indicating the redox reaction occurred between surface adsorbed oxygen and H_2S gas. The S 2p XPS spectra of the NiO arrays film sensor are shown in Figs. 8e and f. The main peak of S 2p at 168.9 eV before the sensor exposure to H_2S corresponds to the binding energy of S-containing components of residual sulphate in the product. The three peaks of S 2p at binding energies of 168.8, 167.2 and 162.1 eV after the sensor exposure to H_2S can be assigned to the characteristic peaks for sulphate, sulfur dioxide and sulphide, respectively. It suggests that the oxidation product of H_2S is SO_2 in this detection process. The existence of SO_2 in the final gaseous product is also confirmed by Gas chromatogram and Mass spectrum analyses after H_2S sensing measurement of the sensor, as shown in Fig. S8.

Based on the above experimental results and reported investigation, NiO nanowall arrays film sensor, exhibiting good gas response to H_2S, might be explained by the following sensing mechanism: As is known to all, NiO is a kind of p-type semiconductor oxides. The operating principle of NiO gas sensors is based on the change in resistance of the arrays film sensor due to the adsorption and desorption process of oxygen molecules on the surface of the NiO. When the sensor is exposed to air, oxygen molecules adsorb onto the surface of the arrays film sensor (Eq. 1) and form chemisorbed oxygen species in the form of O_2^-, O^- or O^{2-} ions at different temperatures (Eq. 2-4) by capturing the conduction band electrons [34]. The ionized adsorption of oxygen leads to the formation of hole-accumulation layers (HALs), and conduction occurs mainly along the near-surface HAL. This leads to the formation of an electronic core-shell configuration [35]. The transfer of electrons to oxygen species results in an increase in the concentration of holes carrier, and therefore, the resistance of the sensor decreases. In the measurement environment of H_2S gas at 92 °C (=365 K), H_2S molecules adsorb onto the sensor surface (Eq. 5) and interact with the pre-chemisorbed oxygen anions (O_2^-) and release a few trapped electrons back to the conduction band of NiO nanowall arrays (Eq. 6). The recombination between the electrons and holes (Eq. 7) results in a decrease in the concentration of surface holes carrier in the NiO arrays, consequently increasing the surface resistance of the sensor. Schematic illustration of the possible mechanism of NiO nanowall arrays to H_2S is shown in Fig. 9.

$$O_2\,(gas) \rightarrow O_2\,(ads) \quad (1)$$

$$O_2\,(ads) + e^- \rightarrow \begin{cases} O_2^-\,(ads)\ (< 420\ K) \\ 2O^-\,(ads)\ (420\text{-}670\ K) \\ O^{2-}\,(ads)\ (> 670\ K) \end{cases} \quad (2)\text{-}(4)$$

$$H_2S\,(gas) \rightarrow H_2S\,(ads) \quad (5)$$

$$2H_2S\,(ads) + 3O_2^-\,(ads) \rightarrow 2SO_2 + 2H_2O + 6e^- \ (365\ K) \quad (6)$$

$$e^- + h^+ \leftrightarrow Null \quad (7)$$

Conclusions

In summary, we demonstrated a simple but high-effective approach for fabricating network-like, hierarchically structured, porous nanowall NiO arrays film in-situ on ceramic tubes for gas sensing. Such NiO sensor exhibited high sensitivity to H_2S (detection limit of 1 ppb) with good selectivity at 92 °C. Even at room temperature, the sensor showed good gas response to H_2S. The air humidity had no influence on this NiO arrays film sensor at low temperature of 92 °C and room temperature. The H_2S-sensing mechanism could be elucidated by a redox reaction between the H_2S molecules and the chemisorbed oxygen ions. The superior H_2S sensing performance could be mainly attributed to the hierarchically porous structure in the unique nanowall arrays with a large specific surface area. We believe that this porous nanowall NiO arrays film sensor is promising for indoor air quality monitoring.

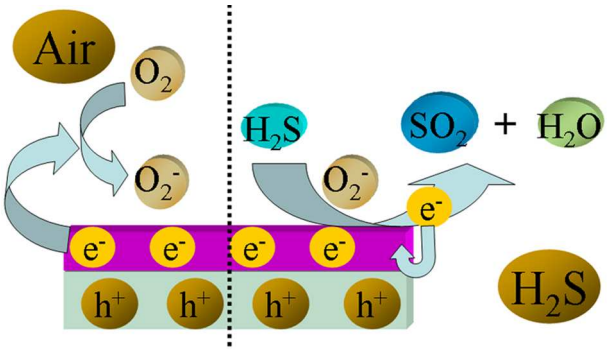

Fig. 9 Schematic illustration of the possible mechanism of NiO nanowall arrays film sensing to H_2S at 92 ºC.

Acknowledgments

This work was financial supported by the National Natural Science Foundation of China (61271126, 21201060 and 21305033), Program for Innovative Research Team in University (IRT-1237), Program for Science and Technology Project of Heilongjiang province (B201101, B201414), Heilongjiang Educational Department (2013TD002, 2011CJHB006, 12531506), Youth Foundation of Harbin (2013RFQXJ142).

References

Key Laboratory of Functional Inorganic Material Chemistry, Ministry of Education, School of Chemistry and Materials Science, Heilongjiang University, Harbin, 150080, China
E-mail: lhhuo68@yahoo.com. Tel /Fax: +86 451 86608426.

† Electronic Supplementary Information (ESI) available. See DOI: 10.1039/b000000x/

1 North Carolina Department of Environment and Natural Resources. http://daq.state.nc.us/toxics/studies/H_2S/. Accessed 2003.
2 Y. Z. Guan, C. G. Yin, X. Y. Cheng, X. S. Liang, Q. Diao, H. Zhang and G. Y. Lu, *Sens. Actuators, B*, 2014, 193, 501-508.
3 E. D. Gaspera, M. Pujatti, M. Guglielmi, M. L. Post and A. Martucci, *Mater. Sci. Eng., B*, 2011, 176, 716-722.
4 R. Tabassum, S. K. Mishra and B. D. Gupta, *Phys. Chem. Chem. Phys.*, 2013, 15, 11868-11874.
5 L. Q. Mai, L. Xu, Q. Gao, C. H. Han, B. Hu and Y. Q. Pi, *Nano Lett.*, 2010, 10, 2604-2608.
6 S. M. Zhang, P. P. Zhang, Y. Wang, Y. Y. Ma, J. Zhong and X. H. Sun, *ACS Appl. Mater. Interfaces*, 2014, 6, 14975-14980.
7 Y. Qin, F. Zhang, Y. Chen, Y. J. Zhou, J. Li, A. W. Zhu, Y. P. Luo, Y. Tian and J. H. Yang, *J. Phys. Chem. C*, 2012, 116, 11994-12000.
8 S. Steinhauer, E. Brunet, T. Maier, G. C. Mutinati, A. Köck, O. Freudenberg, C. Gspan, W. Grogger, A. Neuhold and R. Resel, *Sens. Actuators, B*, 2013, 187, 50-57.
9 G. J. Sun, S. W. Choi, A. Katoch, P. Wu and S. S. Kim, *J. Mater. Chem. C*, 2013, 1, 5454-5462
10 K. I. Choi, H. J. Kim, Y. C. Kang and J. H. Lee, *Sens. Actuators, B*, 2014, 194, 371-376.
11 L. F. He, Y. Jia, F. L. Meng, M. Q. Li and J. H. Liu, *J. Mater. Sci.*, 2009, 44, 4326-4333.
12 S. J. Choi, C. Y. Choi, S. J. Kim, H. J. Cho, M. Hakim, S. Jeon and I. D. Kim, *Scientific Reports*, 2015, 5, 1-9.
13 K. Yao, D. Caruntu, Z. M. Zeng, J. J. Chen, C. J. O'Connor and W. L. Zhou, *J. Phys. Chem. C*, 2009, 113, 14812-14817.
14 C. H. Wang, X. F. Chu and M. M. Wu, *Sens. Actuators, B*, 2006, 113, 320-323.
15 Y. Du, W. N. Wang, X. W. Li, J. Zhao, J. M. Ma, Y. P. Liu and G. Y. Lu, *Mater. Lett.*, 2012, 68, 168-170.
16 P. Rai, J. W. Yoon, H. M. Jeong, S. J. Hwang, C. H. Kwak and J. H. Lee, *Nanoscale*, 2014, 6, 8292-8299.
17 F. Li, Y. J. Chen and J. M. Ma, *RSC Adv.*, 2014, 4, 14201-14205.
18 L. Xu, R. F. Zheng, S. H. Liu, J. Song, J. S. Chen, B. Dong and H. W. Song, *Inorg. Chem.*, 2012, 51, 7733-7740.
19 C. Luyo, R. Ionescuc, L. F. Reyes, Z. Topalian, W. Estrada, E. Llobet , C. G. Granqvist and P. Heszler, *Sens. Actuators, B*, 2009, 138, 14-20.
20 X. L. Cheng, Z. M. Rong, X. F. Zhang, Y. M. Xu, S. Gao, H. Zhao and L. H. Huo, *Sens. Actuators, B*, 2013, 188, 425-432.
21 Z. S. Hosseini, A. Iraji zad and A. Mortezaali, *Sens. Actuators, B*, 2015, 207, 865-871.
22 X. H. Wang, L. Qiao, X. L. Sun, X. W. Li, D. K. Hu, Q. Zhang and D. Y. He, *J. Mater. Chem. A*, 2013, 1, 4173-4176.
23 Y. Qian, R. Liu, Q. F. Wang, J. Xu, D. Chen and G. Z. Shen, *J. Mater. Chem. A*, 2014, 2, 10917-10922.
24 L. L. Sui, Y. M. Xu, X. F. Zhang, X. L. Cheng, S. Gao, H. Zhao, Z. Cai and L. H. Huo, *Sens. Actuators, B*, 2015, 208, 406-414 .
25 M. Vidotti, R. P. Salvador and S. I. C. Torresi, *Ultrason. Sonochem.*, 2009, 16, 35-40.
26 M. W. Louie and A. T. Bell, *J. Am. Chem. Soc.*, 2013, 135, 12329-12337.
27 Y. Jiang, D. D. Chen, J. S. Song, Z. Jiao, Q. L. Ma, H. J. Zhang, L. L. Cheng, B. Zhao and Y. L. Chu, *Electrochim. Acta*, 2013, 91, 173-178.
28 H. W. Wang, H. Yi, X. Chen and X. F. Wang, *Electrochim. Acta*, 2013, 105, 353-361.
29 M. A. Peck and M. A. Langell, *Chem. Mater.*, 2012, 24, 4483−4490.
30 C J. F. Moulder, Handbook of X-ray photoelectron spectroscopy: a reference book of standard spectra for identification and interpretation of XPS data, Published by Perkin-Elmer Corporation, Physical Electronics Division, USA, 1992.
31 Y. F. Wang, F. D. Qu, J. Liu, Y. Wang, J. R. Zhou and S. P. Ruan, *Sens. Actuators, B*, 2015, 209, 515-523.
32 M. Tomellini, *J. Electron Spectrosc. Relat. Phenom.*, 1992, 58, 75-78.
33 F. H. Su, X. M. Lv and M. H. Miao, *Small*, 2015, 11, 7, 854-861.
34 M. E. Franke, T. J. Koplin and U. Simon, *small*, 2006, 2, 36-50.
35 H. J. Kim and J. H. Lee, *Sens. Actuators, B*, 2014, 192, 607-627.

Highly sensitive H_2S detection sensor at low temperature based on hierarchically structured NiO porous nanowall arrays

Tingting Yu, Xiaoli Cheng, Xianfa Zhang, Lili Sui, Yingming Xu*, Shan Gao, Hui Zhao, Lihua Huo*

Key Laboratory of Functional Inorganic Material Chemistry, Ministry of Education, School of Chemistry and Materials Science, Heilongjiang University, Harbin, 150080, China; Tel /Fax: +86 451 86608426;

E-mail address:lhhuo68@yahoo.com

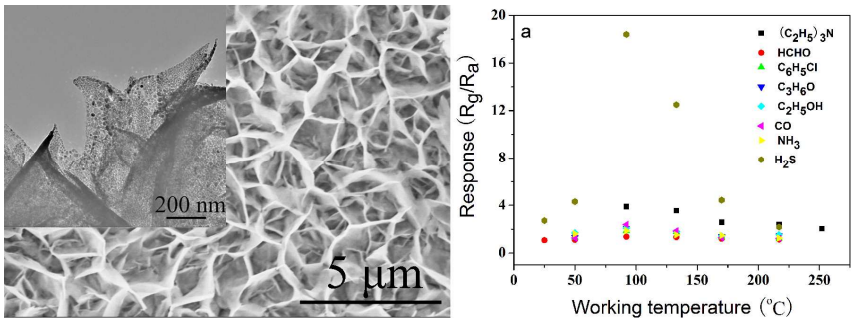

NiO porous nanowall arrays have been successfully in-situ growth on the ceramic tube by hydrothermal reaction, combined with calcined process. With such unique hierarchical pore, the arrays film sensor displayed excellent sensing performance toward H_2S.